Bandwidth Reduced Full-Wave Simulation of Lossless and Thin Planar Microstrip Circuits

A. Caproni, F. Cervelli, M. Mongiardo, L. Tarricone, F. Malucelli

Istituto di Elettronica, Via G. Duranti,93, 06131, Perugia, Italy.
Corresponding Author: L. Tarricone, tarricone@istel.ing.unipg.it

Abstract— **We present a full-wave, high-performance, numerical scheme for the analysis of planar microstrip circuits which is based on an efficient electromagnetic formulation of the field problem and on the bandwidth reduction of the discretized sparse matrix.**

The above mentioned electromagnetic efficiency is attained by considering a Mixed Potential Integral Equation (MPIE) with the kernel expressed by closed-form spatial-domain Green's functions; as a consequence, the reaction integrals are evaluated by using just one-dimensional numerical integration over a finite spatial domain. Moment method discretization of the MPIE leads to the corresponding matrix problem.

The accurate analysis of the matrix properties shows that a sparsity of 70-85 % in the discretized linear system can be routinely enforced without significantly altering the solution accuracy.

A new scheme for the sparse matrix bandwidth reduction, particularly tailored for electromagnetic problems, can be therefore introduced, leading to considerable reductions of the simulation time. Results are presented demonstrating that the use of a bandwidth reduction strategy coupled with efficient problem-matched Green's functions allows as to obtain speed-ups in simulation time of more than one order of magnitude with respect to standard state-of-the-art implementations.

I. Introduction

The efficient and rigorous analysis of microstrip circuits, including patch antennas and printed dipoles, requires the use of appropriate Green's function representation, adequate choice of basis functions for field expressions, and, last but not least, efficient strategies for the solution of the linear system resulting from the integral equation discretization.

Recently, by means of an ingenious device, a novel approach has been developed [1] for obtaining closed-form expressions for the spatial domain Green's functions corresponding to the vector and scalar potentials associated with a horizontal electric dipole located over a tick substrate. The technique has been furtherly extended in [2], [3] and leads to substantial savings of computation time when analizing planar microstrip configurations by variational techniques, such as the method of Moments (MoM). In this work we have therefore used the latter Green's functions, hence significantly reducing the amount of time necessary for the impedance matrix filling.

Concerning the choice of suitable basis functions, although it has been shown in several occasions that the inclusion of the appropriate edge singularity significantly enhances convergence properties [4], in order to keep the geometries as flexible as possible, standard roof-top expansions have been used.

However, the suitable selection of problem-matched Green's functions and therefore the efficient computation of the impedance matrix, although of primary relevance from the electromagnetic viewpoint, is only a part of the procedure necessary in order to solve the field-problem in microstrip stuctures.

II. The Electric Field Mixed Potential Integral Equation for Microstrip Structures

A. MPIE Solution with the MoM and Closed Form Green's Functions

We consider N-port planar circuits, similar to that sketched in Fig. 1, with infinite transverse dimensions for both the dielectric and the ground plane; the metalization thickness is assumed negligeable.

In order to achieve improved convergence properties, we select Mixed Potential Integral Equations (MPIE) [5], [6], [7], which are solved by considering closed-form Green's functions in the spatial domain and by using the method of moments (MoM). The relative electric field integral equation is derived from the Leontovich boundary condition as:

$$\mathbf{n} \times [\mathbf{E^e} + \mathbf{E^s}] = \mathbf{Z_S}[\mathbf{n} \times \mathbf{J_S}] \tag{1}$$

where $\mathbf{E^e}$ and $\mathbf{E^s}$ denote respectively the excitation and scattered electric field, and $\mathbf{Z_s}$ and $\mathbf{J_S}$ denote the surface impedance and electric current density respectively.

The electric field is written as a function of the vector potential $\mathbf{A}$ and the scalar potential ϕ, which satisfy the Helmholtz vector and scalar equations, respectively:

$$\mathbf{E} = -\mathbf{j}\omega\mathbf{A} - \nabla\phi \tag{2}$$

By introducing the Green's functions $\bar{\bar{\mathbf{G}}}^{\mathbf{A}}$ and G^q for the surface electric current density $\mathbf{J_S}$ and for the surface electric charge density q_S, respectively, a Fredholm integral equation of the first kind is obtained, solvable by the MoM after suitable Green's function evaluation.

Spatial domain mixed potential Green's functions for a layered medium are expressed by Sommerfeld integrals [8] whose integrands are slowly decaying obscillating functions, hence the calculation is very time-consuming. A possible approach to circumvent this problem is the quasi-dynamic image model [9], which is not accurate enough when surface and leaky wave effects must be accounted for [10]. An ingenious device to evaluate the above mentioned Green's functions in closed form was first suggested in [1] for single-layer problems, and extended more recently to multilayer structures [2], [3]. The latter is adopted in this work.

The integral equations are solved using the Galerkin's MoM, i.e. by selecting the same functions for tests and exapnsion [11]. This way, a linear system of size N is derived from the MPIE:

$$\begin{bmatrix} Z_{xx} & Z_{xy} \\ Z_{yx} & Z_{yy} \end{bmatrix} \begin{bmatrix} I_x \\ Iy \end{bmatrix} = \begin{bmatrix} V_x \\ Vy \end{bmatrix} \tag{3}$$

The entry Z_{ij} in the impedance matrix represents the tangential electric field generated by the j-th basis function and weighted by the i-th test one. This entry is expressed by a four-fold integral, in the spatial variables x', y' -corresponding to the source coordinates- and x, y -corresponding to the test coordinates. Part of its evaluation can be performed analytically [12] and, by paying attention to the choice of appropriate basis functions, the integrals *"can be reduced to double integrals over finite domains"* [13]. Thanks to the circular symmetry of mixed potential Green's functions, with appropriate changes into polar variables, in this work they are reduced to a simple integral in the variable r (representing the distance between source and probe):

$$\begin{aligned}
Z_{xx} &= \int \left[W_{1\,x}(r) G^A_{xx}(r) - \frac{1}{\omega^2} W_{2\,x}(r) G^q(r) \right] r\, dr \\
Z_{xy} &= \int \left[-\frac{1}{\omega^2} W_{3\,x}(r) G^q(r) \right] r\, dr \\
Z_{yx} &= \int \left[-\frac{1}{\omega^2} W_{3\,y}(r) G^q(r) \right] r\, dr \\
Z_{yy} &= \int \left[W_{1\,y}(r) G^A_{yy}(r) - \frac{1}{\omega^2} W_{2\,y}(r) G^q(r) \right] r\, dr
\end{aligned} \tag{4}$$

The unknowns I_x and I_y are the (complex) amplitudes of the basis functions. The right-hand-side (rhs) vector $[V]$ depends on the excitation applied to the microstrip network.

During the simulations two sources have been used: the series voltage-source and the coaxial cable probe, which has been modelled using suited surface current distributions [14]. Using the voltage source the rhs vector is quickly filled in, as many of its terms are nulls. Both sources, voltage source and coaxial probe, give the same numerical results.

B. De-embedding Technique

The method described till now is well-suited in order to evaluate the electric current distribution on the conducting plane. Further elaborations are needed for calculating the scattering parameters of the multiport equivalent network. To this end, the latter network is analized N times, each time applying the source to a different input port and leaving open the remaining ports. Accordingly, a linear system of size N^2 is attained, exhibiting as unknowns the scattering parameters at the various ports [15]. The terminal-plane locations are chosen sufficiently far away from the discontinuities, so that only the fundamental mode propagates. In this way, we evaluate the propagation constant β_i and the complex amplitudes of the incident (a_i) and reflected (b_i) fundamental mode by considering the current samples observed at regular intervals along the center section of the line (de-embedding section), as shown in Fig. 2. The choice of an appropriate de-embedding section, and its distance from discontinuities, is performed with suitable heuristical procedures, taking into account the circuit parameters and dimensions. If the source is applied on a port, it is positioned at the end of the line, otherwise the microstrip termination is left open, and the length of this line is selected so as to allow vanishing of the evanescent modes.

The de-embedding technique is based on Prony's method [16]: the longitudinal electric current is known in $2M_s$ sample points, and is approximated with a sum of M_s complex exponentials:

$$I(x_n) \approx \sum_{m=1}^{M_s} A_m e^{\gamma_m n \Delta x} \qquad per\ n=1,...N \tag{5}$$

The amplitudes of forward and backward waves can be evaluated from A_m terms. By applying this procedure to every line connecting the network with the remaining part of the circuit in the N possible configurations, the final linear system is built, allowing the evaluation of the network scattering parameters.

C. Code Testing

In order to demonstrate the reliability of the implemented code, we illustrate now some results which compare the theoretical analysis of some circuits. In Fig. 3 the results relative to a stub with a substrate thickness of $d = 1.27mm$ and $\varepsilon_r = 10.65$ are shown and compared with experimental results [17]. In Fig. 4 the above presented technique has been applied to characterize a microstrip double-stub discontinuity; the matching section is printed on a 10 mil substrate of relative permittivity 9.9: the magnitude and phase of the scattering parameters are compared to measurement from [18]. As illustrated, the agreement for magnitude and phase is excellent; in particular, the agreement of the phase is within 4° across the considered frequency range.

Similar results can be obtained also at a fraction of the numerical effort, by exploiting the numerical properties (i.e. the sparsity and the bandwidth reduction scheme) of the discretized matrix, as discussed in the next sections.

III. The Impedance Matrix

In the previous sections we have described the MPIE, which, discretized via MoM, is suited for the efficient simulation of arbitrarily-shaped microstrip structures. In this section, we investigate the main numerical characteristics of the approach, in order to enhance its numerical efficiency. We will point out that the use of appropriate strategies in the domain partitioning and, above all, in the solution of linear systems, when coupled with effective approaches for matrix permutation, enables considerable speed-ups without significantly affecting the accuracy of the simulation.

A. Preliminary Observations

The MPIE approach is well-suited to simulate circuits with arbitrary shapes, thanks to the partitioning of the microstrip lines into elementary rectangular cells. The simulation accuracy can also be increased by reducing the size of the elementary cells, so as to better approximate the metalization contour. A quite significant number of basis functions are needed in such a case, with a consequent increase of the computing time needed to evaluate the system matrix and to solve the MoM system (3). These two steps (system generation and solution) do not generally require the same amount of time: the linear system solution is often much more time-demanding, its complexity depending on the problem size N_s as a function N_s^α, with $2 < \alpha < 3$; on the contrary, the matrix evaluation has a linear dependence with the number of unknowns N_s.

The matrix entries' computation has been enhanced by exploiting some geometrical properties of the problem. Thanks to the radial symmetry of Green's functions, several matrix entries are identical; in addition the matrix has a particular pattern, similar to a Toeplitz one. Moreover, the electromagnetic interaction between basis and test functions generally decreases for increasing distances; their reaction term is significantly smaller than those appearing in the main diagonal. Therefore, a threshold distance value, d_c, can be found so that all the terms corresponding to the interactions for a distance greater than d_c can be omitted.

B. Properties of the System Matrix

In order to enhance the system solution time, as detailed in the following section, it has been quite useful to investigate the numerical properties of the system matrix entries in (3). Some examples are proposed (Figures 5,6), showing the matrix patterns (viz. the zero-non-zero structure) resulting for different circuit layouts. From Figures 5,6 it is also apparent where the most significant entries (with higher values) are positioned in the matrix; in these figures, the gray levels are related to the magnitude of the matrix entry: a black entry has a larger absolute value than a gray one, while values smaller than 10^{-9} have always been omitted.

Figures 5,6 clearly show that generally a few entries are significantly larger than the remaining ones, hence retaining an amount of information significant enough in order to accurately solve the problem. Therefore, the basic idea of this numerical analysis is the evaluation of the effects of a thresholding action on the matrix entries. We hence consider the following question: *for a fixed threshold v_t, so that every entry smaller than v_t is neglected, how is the numerical accuracy perturbed?* As we will see in the following, the answer to the question above will pave the way to the introduction of a bandwidth reduction scheme which substantially decreases the system solution time.

As observed from Figures 5,6, when increasing the threshold value v_t, the percentage of "zero" entries (i.e. the *sparsity* S) grows up, the non-zero positions actually depending on the circuit shape. More specifically, they are a consequence of the numbering scheme used to order the basis functions.

However, also other parameters affect the system matrix pattern: the frequency, the substrate thickness, the dielectric constant, and the elementary cell's size. We evaluate the percentage of "significant entries" in the system matrix at the highest operating frequency, which is the most critical one.

As shown in the tables in Figures 5,6, for different v_t the sparsity S of the system matrix has been computed, as well as the relative error on the system solution, and the consequent maximum error on the propagation constants and on the scattering parameters. These computations have been performed with a 7-decimal-digit notation. It can be observed that the propagation constant, being a variational quantity, is almost not affected by the thresholding action. In other words, Prony's method is more robust in the exponent evaluation, rather than in the evaluation of the complex amplitudes of the exponential functions. Finally, it can also be noticed that a direct relationship exists between v_t and the error in the system solution, whilst the link between v_t and the error affecting the scattering parameters is less straightforward. Anyway, with a threshold $v_t = 10^{-5}$, the maximum observed error on the scattering parameters is generally less than than 3%, therefore comparable with experimental errors. For such a v_t, the sparsity is generally $70\% < S < 85\%$, depending however on the microstrip circuit topology, and on the physical parameters (frequency, substrate thickness and permittivity).

IV. Bandwidth Reduced Solution of the Linear System

The analysis performed in the previous sections demonstrates that the linear system (3) is not necessarily dense: when an appropriate threshold v_t is chosen,

so that the system matrix entries smaller than v_t are neglected, the matrix pattern becomes sparse. Of course, this implies some rounding errors, which, nonetheless, allow to achieve a substantial reduction of the simulation time.

A. The Impedance Matrix Sparse System Solution

A sparse system can be solved by using iterative methods (such as biconjugate-gradient algorithms), or direct sparse solvers, which are not always robust. The latter perform an LU-factorization and a backsubstitution solution; dealing with sparse matrices, this can lead to the so-called "fill-in" problem [19], i.e. the risk of obtaining dense LU factors, with a high degradation of performance. This problem is not encountered using banded direct solvers, i.e. solvers suited to systems with a banded matrix. Therefore, the effective choice for an efficient and robust solution of the system is either iterative algorithms or banded direct solvers.

The numerical complexity of both the above mentioned approaches is well-known, and is $o(NZ)$ for iterative methods (with NZ equal to the number of non-zero entries in the matrix) and $o(BN^2)$ for banded algorithms (with BN equal to the matrix bandwidth) [19]. Therefore, a straight implementation of a banded solver is generally less efficient than using an iterative solver: the system matrix, as observed in the previously shown example, generally exhibits a large bandwidth.

B. Bandwidth Reduction of the Impedance Sparse Matrix

It is worthwhile to note that some manipulations can be performed on the matrix pattern by using straightforward matrix algebra; in fact, the linear system

$$\mathbf{Ax} = \mathbf{B} \tag{6}$$

has the same numerical properties of the transformed system

$$(\mathbf{P^T AP})(\mathbf{P^T x}) = \mathbf{P^T B} \tag{7}$$

where $\mathbf{P}$ is a permutation matrix. This new system (7) has an interesting property: depending on the appropriate choice of the permutation matrix $\mathbf{P}$, it can be transformed into one with a minimum bandwidth. Once the optimum permutation matrix is found, the efficiency of the linear system solver is considerably enhanced by using a banded direct solver, and orders of magnitudes of speed-ups can be observed.

Moreover, an efficient use of direct banded solver is attractive for two more reasons: in practical applications, when we need to evaluate the dispersion curve at several frequency points, the optimum permutation as evaluated at the maximum frequency in the working range is also well-suited to every other frequency; secondly, when the same system has to be solved for different rhs, the factorization step can be performed just once, and only the backsubstitution step is repeated for every different rhs, this making direct solvers preferrable to iterative ones.

C. Methods for Bandwidth Reduction

In the past several different approaches have been presented for the evaluation of the optimum numbering of rows and columns of the $\mathbf{A}$ matrix so as to attain a minimum bandwidth [19], [20], [21], [22]. One of the most effective approaches specifically devoted to bandwidth reduction is that derived from the Cuthill-McKee (CM) method [20], [21].

The main idea of this class of algorithms is related to the graph representation of the matrix. Let us consider the matrix$\mathbf{A}$ with a symmetric zero-non-zero pattern . A so-called "incidence" graph can be easily associated to the latter matrix, as in Fig. 7, where each row/column is represented by a node, and nodes i and j are connected each other if and only if the entry a_{ij} is not a null. The incidence graph can be partitioned into "levels", as shown in the same picture. All the nodes with the same "distance" from the graph's root are included in the same level. It can be intuitively understood (and this is demonstrated in [23]) that the larger the number of levels in an incidence graph, the smaller the bandwidth of the matrix. Therefore, the goal is to find out a node numbering scheme that maximizes the number of levels in the incidence graph.

The basic items of bandwidth reduction algorithms, while being quite well-known to those acquainted with bandwidth reduction and graph partitioning, are not trivial, and can be summarized as:

- partitioning phase: select a new root node for the incidence graph, and cut some edges, such that there are edges only between nodes belonging to the same level, or to two adjacent levels
- numbering phase: number the nodes by increasing level, and inside each level number them according to a particular criterion.

Starting from these ideas, a new approach (called WBRA) has been proposed by the authors in [24], [25], implementing some improved features and enhancing the performance of bandwidth reduction and computing times quite substantially. The WBRA's main new features can be summarized in the following way:

- partitioning phase: the graph is divided into levels so that the minimum number of nodes belong to the same node (in fact, the bandwidth is directly affected by the size of the largest subset). Differently from the CM approach, the WBRA approach introduces some heuristic criteria specifically devoted to this goal
- numbering phase: the WBRA algorithm applies the numbering to a set of "promising" level structures determined during the partitioning phase. Some advanced (and rather complex) heuristic criteria are then used to select the best level partitioning and numbering in an efficient way. Differently from CM approach, WBRA explores different level structures, this allowing better performance.

A simple example of the final matrix, level structure and incidence graph for a sparse matrix is shown in Fig.

8. It can be easily observed that, starting from the incidence graph in Fig. 7, if node 3 is transformed into node 1, node 1 into 2, 4 into 3, and 2 into 4, the graph of Fig. 8 and its companion matrix are obtained. The corresponding P is

$$\begin{bmatrix} 0 & 0 & 1 & 0 \\ 1 & 0 & 0 & 0 \\ 0 & 0 & 0 & 1 \\ 0 & 1 & 0 & 0 \end{bmatrix}$$

V. Results

We present numerical results demonstrating the high-performance of the approach for two cases: a 2-port circuit (a double stub), and a 4-port one (a branch coupler). All the reported simulations have been run on an entry level workstation, with a 32MB RAM. The use of a strategy for reducing the numerical complexity of the problem (the thresholding), coupled with a state-of-the-art method for bandwidth reduction of the system matrix in (3), highly enhance the performance of the code. The results compare the performance of the approach in three different possible scenaries:

- No thresholding is performed, a dense solver (Gauss-Jordan, GJ) is used in the (3)
- Thresholding is performed with a fixed v_t, and an iterative sparse solver (biconjugate-gradient, BCG) is used
- Thresholding is performed with a fixed v_t, and the bandwidth of the system matrix minimized using WBRA. A banded solver (BN) is then used in the (3)

All the three linear system solvers (GJ, BCG, and BN) are selected from SLATEC public-domain collection. The iterative sparse solver is generally used with 100-180 iterations, so that an error of 10^{-9} is achieved (this value is enough to guarantee an appropriate convergence also when a thresholding is performed). The threshold value, as discussed in section 6.2, is 10^{-5}.

The computation is divided into two main tasks: the time necessary to evaluate the matrix and the rhs in the (3) (we call this step "system generation"), and the time to solve the same system. When the GJ approach is used, every frequency point is simulated with the same computing time. In the BCG and BN case, this is not true. The first frequency point (the upper limit in the frequency range) is used to determine the matrix entries which are smaller than v_t, and need not to be computed at next frequency steps. Moreover, in the BN case, also the permutation matrix **P** so that the bandwidth is reduced, is computed, and the system rearrangement performed as suggested in (7). Therefore, in the BCG and BN case, the first frequency point analysis is slower than the following ones.

A. 2-Port Network

The two-port network represented in Fig. 5 has been simulated in the range 2.5-3.5 GHz. The dielectric constant is 2.6, and the cell dimension is 3mm (uniform meshing with square cells). The system size in (3) is 220. In Table II we show the performance results for the main tasks. Times to perform the tasks (system generation, solution, and bandwidth reduction) are given in seconds. An IBM RS6000 250 T, an entry level workstation, has been used. Times in Table I refer to a single frequency point. Times for the system generation for the BCG and BN case suppose that the thresholding on the matrix entries has already been performed. As previously discussed, this can not be assumed for the first frequency point. In that case, the system generation is performed in 53 s for the GJ case, and in 44 s in the BCG and BN cases.

Table I: Times for the different tasks (in seconds) for one frequency point.

Method	*System Gen*	*System Sol.*	*Bandwidth .Red.*
GJ	53	4.5	-
BCG	11.9	3	-
BN	11.9	0.2	0.5

The sparse matrix solved with BCG is obtained with a 10^{-5} threshold, and its bandwidth is 208. Using WBRA it is reduced to 72. It must also be observed that the system (3) solution is repeated for each frequency point as many times as the number of ports, in order to evaluate the scattering parameters.

In Table II the timings for a complete frequency analysis (100 frequency points) are presented for the three methods. Remember that if the first frequency point is the upper-frequency one, the bandwidth minimization can be performed only once (as previously discussed in section 6.2).

Table II: Times (in seconds) for 100 frequency point.

Method	*Upper Freq. Point*	*Remaining 99 Freq. Points*	*Total Time*
GJ	62	6138	6200
BCG	50	1772	1832
BN	45	1198	1243

It can be seen that a global speed-up of more than 3 times is attained with the BCG strategy, and of around 5 with the BN+WBRA strategy. This is due to the huge performance improvement obtained in the linear system solution. Using the thresholding, the BCG solves the sparse system in around 3s instead of 4.5s (dense GJ). The BN solver, after the bandwidth minimization (which takes 0.5 s) performs the solution in 0.2s. Moreover, the banded solver is a direct LU algorithm. As stressed before, for each frequency point the system is solved as many times as the ports are (this case 2 times) with different rhs. This means that using the banded solver the only backsubstitution step is performed twice, and it is quite well known that this step is very fast, compared with the LU factorization step.

The improvement in the efficiency is obtained without degradating too much the accuracy of the simulation: both the BCG and the BN strategy affect the result with an error of around 3%, as already shown in the table in Fig. 5. This is quite satisfactory, and still comparable with experimental errors.

B. 4-Port Network

The results for the 4-port coupler of Fig. 6 are presented following the same logical path of the previous section: the GJ, BCG and BN strategy are compared, demonstrating the superior performance of the BN+WBRA strategy. As the number of ports is increased in this example, very substancial speed-ups are achieved.

The circuit is studied in the range 2.5-3.5 GHz, with a substrate with $\varepsilon = 2.6$, and square cell size of edge 3mm. In Table III results are shown, with times in seconds referred to the above mentioned IBM 250 T. Data do not refer to the first frequency point (upper limit of the range). In that case, the system is generated in 111.4 s with the GJ approach, and in 81 s with the BCG and BN one. The system size is 401.

Table III: Times for the different tasks (in seconds) for one frequency point.

Method	*System Gen.*	*System Sol.*	*Bandwidth Red.*
GJ	111.4	57	-
BCG	15.4	7.4	-
BN	15.4	0.6	2

In this case, the bandwidth of the sparse matrix obtained performing a thresholding with $v_t = 10^{-5}$ is 310, and by applying the WBRA it is reduced to 82, with a huge enhancement in the solution time when the BN solver is used. For the coupler, the speed-ups for a 100-point frequency curve are very interesting, as the system solution is repeated 4 times for each frequency point, and a direct LU banded solver is extremely suited and effective. Table IV demonstrates this, showing the total times for the whole frequency analysis:

Table IV: Times (in seconds) for 100 frequency point.

Method	*Upper Freq. Point*	*Remaining 99 Freq. Points*	*Total Time*
GJ	338.6	33521	33860
BCG	141	4356	4497
BN	112.2	1723	1835

It can be seen that the BCG strategy is more than 7 times faster than the standard implementation of the MPIE approach solved with the MoM. A strategy based on WBRA for bandwidth reduction and a BN solver is more than 18 times faster. Also in this case, the error in the solution is around 3% (see the table in Fig. 6) on the computed scattering parameters.

This last example demonstrates that on increasing the number of ports, and the complexity of the circuit layout, the proposed strategy becomes more and more high-performing.

VI. Conclusions

An efficient electromagnetic and numerical approach has been proposed for the analysis of arbitrarily-shaped microstrip circuits, based on the solution of the Mixed-Potential Integral Equations via Method of Moments. The use of analytically evaluated closed-form Green's functions and general de-embedding techniques makes the code efficient from the electromagnetic view-point.

A detailed analysis of the resulting linear system, which solution represents one of the key-issues in the code performance, has demonstrated that, even for standard rooftop basis functions, at the cost of small degradation of the solution accuracy, the generally dense linear system can be reduced to a sparse one, with a sparsity generally in the range 70-85%.

The use of a method for the bandwidth reduction of sparse matrices developed by the authors, while outperforming the previously proposed approaches for bandwidth reduction, when coupled with a banded direct solver, is shown to produce a substantial speed-up in the numerical simulation of microstrip circuits. A speed-up of 5 times has been achieved on a 2-port circuit, and of 18 times on a 4-port circuit.

References

[1] Y. L. Chow, J. J. Yang, D. G. Fang and G. E. Howard, "A closed-form spatial Green's function for thick microstrip substrate", *IEEE Trans. Microwave Theory Tech.*, vol. 39: pp. 588–592, Mar. 1991.

[2] M. I. Aksun and R. Mittra, "Derivation of closed-form Green's functions for a general microstrip geometry", *IEEE Trans. Microwave Theory Tech.*, vol. 40: pp. 2055–2062, Nov. 1992.

[3] G. Dural and M. I. Aksun, "Closed-form Green's functions for general sources and stratified media", *IEEE Trans. Microwave Theory Tech.*, vol. 43: pp. 1545–1552, Jul. 1995.

[4] T. Rozzi and M. Mongiardo, *"Open electromagnetic waveguides"* , IEE, London, 1997.

[5] J. R. Mosig and F. E. Gardiol, "Analytical and numerical techniques in the Green's function treatment of microstrip antennas and scatterers", *Proc. Inst. Elec. Eng., pt. H: Microwave Optics Antennas*, vol. 130: pp. 175–182, 1983.

[6] J. R. Mosig and F. E. Gardiol, "General integral equation formulation for microstrip antennas and scatterers", *Proc. Inst. Elec. Eng., pt. H: Microwave Optics Antennas*, vol. 132: pp. 424–432, Dec. 1985.

[7] J. R. Mosig, "Arbitrarly shaped microstrip structures and their analysis with a mixed potential integral equation", *IEEE Trans. Microwave Theory Tech.*, vol. 36: pp. 314–323, Feb. 1988.

[8] A. Sommerfeld, *"Partial Differential Equations in Physics"*, Academic Press, New York, 1949.

[9] Y. L. Chow, "An approximate dynamic spatial Green's function in three dimensions for finite length microstrip lines",*IEEE Trans. Microwave Theory Tech.*, vol. 28: pp. 393–397, 1980.

[10] J. R. Mosig and F. E. Gardiol, "A dynamical radiation model for microstrip structures". In *Advanced in Electronics and Electron Physics*, vol. 59: pp. 175–182. London Academic Press, 1982.

[11] R. F. Harrington, *"Field Computation by Moment Method"*, Macmillan, New York, 1968.

[12] L. Barlatey, J. R. Mosig and T. Sphicopoulos, "Analysis of stacked microstrip patches with a mixed potential integral equation", *IEEE Trans. Microwave Theory Tech.*, vol. 38: pp. 608–615, May 1990.

[13] M. I. Aksun and R. Mittra, "Estimation of spurious radiation from microstrip etches using closed-form Green's functions", *IEEE Trans. Microwave Theory Tech.*, vol. 40: pp. 2063–2070, Nov. 1992.

[14] J. R. Mosig, "Integral Equation Technique". In *Numerical Techniques for Microwave and Millimeter Wave Passive Structures*, chapter 3. T. Itoh, New York, 1986.

[15] I. Park, R. Mittra and M. I. Aksun, "Numerically efficient analysis of planar microstrip configurations using closed-form Green's functions", *IEEE Trans. Microwave Theory Tech.*, vol. 43: pp. 394–400, Feb. 1995.

[16] R. C. Hall and J. R. Mosig, "The analysis of arbitrarly shaped aperture-coupled patch antennas via a mixed-potential integral equation", *IEEE Trans. Antennas Propagat.*, vol. 44: pp. 608–614, May 1996.

[17] R. Jackson, "Full-wave finite element analysis of irregular microstrip discontinuities", *IEEE Trans. Microwave Theory Tech.*, vol. 37: pp. 81–89, Jan. 1989.

[18] W. P. Harokopus and P. B. Katehi, "Characterization of microstrip discontinuities on multilayer dielectric substrates including radiation losses ", *IEEE Trans. Microwave Theory Tech.*, vol. 37: pp. 2058–2066, Dec. 1989.

[19] I. S. Duff, A. M. Erisman and J. K. Reid, *Direct methods for sparse matrices*. Oxford University Press, 1986.

[20] E. Cuthill and J. McKee, "Reducing the bandwidth of sparse symmetric matrices", in *ACM National Conference*, New York 1969.

[21] N. E. Gibbs, W. G. Poole and P. K. Stockmeier, "An algorithm for reducing the bandwidth and profile of sparse matrix", *SIAM Journal of Numerical Analysis* vol. 13(2): pp. 236–250, 1996.

[22] G. Dueck and J. Jeffs, "A heuristic bandwidth reduction algorithm". *Journal of Combinatorial Mathematics and Combinatorial Computing*, vol 18: pp. 97–108, 1995.

[23] D. Kuo and G. J. Chang, "The profile minimization problem in trees", *SIAM Journal on Computing* vol. 23(1): pp. 71–81, 1994.

[24] A. Esposito, S. Fiorenzo Catalano, F. Malucelli and L. Tarricone, "Sparse matrix bandwidth reduction: algorithms, applications and real industrial sases in electromagnetics", in *High performance Algorithms for Structured Matrix Problems*, ABLEX , Norwood, NJ 1997 (forthcoming).

[25] A. Esposito, S. Fiorenzo Catalano, F. Malucelli and L. Tarricone, "A wonderful bandwidth matrix reduction algorithm", to appear in *Operations Research Letters*, 1997.

[26] M. I. Aksun and R. Mittra, "Choices of expansion and testing functions for the method of moments applied to a class of electromagnetic problems", *IEEE Trans. Microwave Theory Tech.*, vol. 41: pp. 503–508, Mar. 1993.

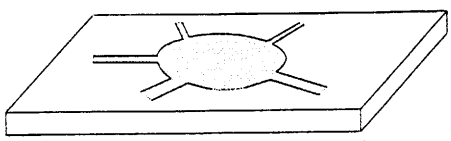

Fig. 1. A general microstrip structure.

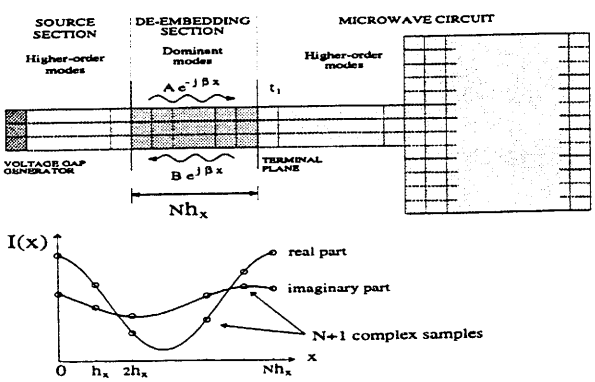

Fig. 2. De-embedding section.

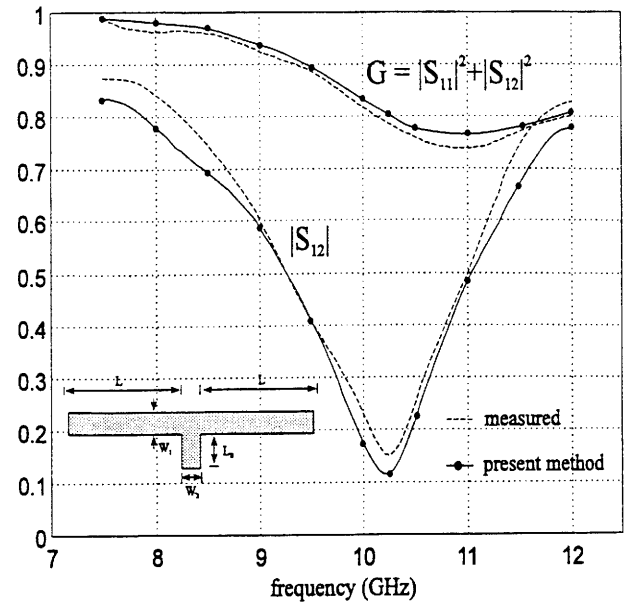

Fig. 3. Scattering parameters for microstrip stub ($W_1 = W_2 = 1.44mm$, $L = 2.16mm$, $\varepsilon_r = 10.65$, $h = 1.27mm$)

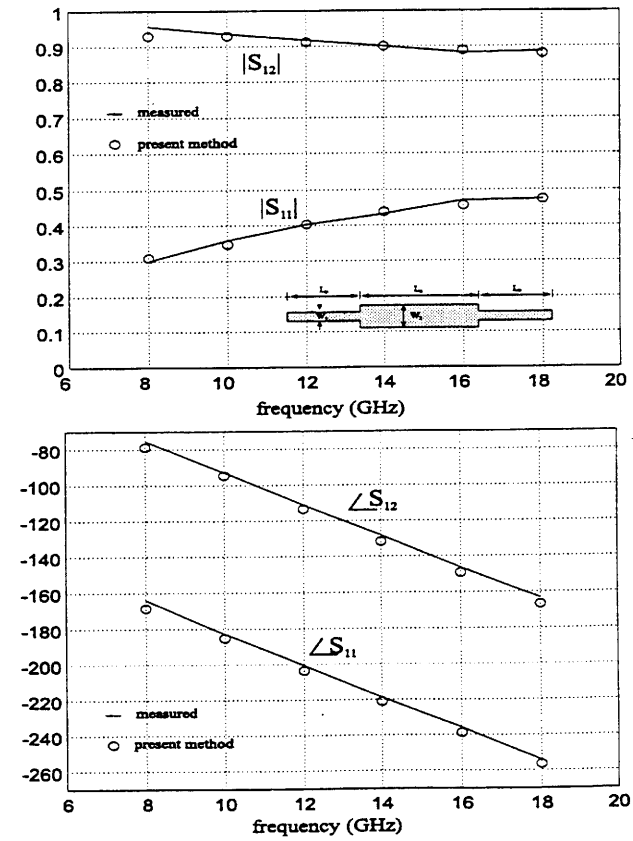

Fig. 4. Magnitude and phase of the scattering parameters for microstrip double-stub ($L_P = 30mil$, $L_S = 50.6mil$, $W_1 = 9.2mil$, $W_2 = 23mil$, $\varepsilon_r = 9.9$, $h = 10mil$)

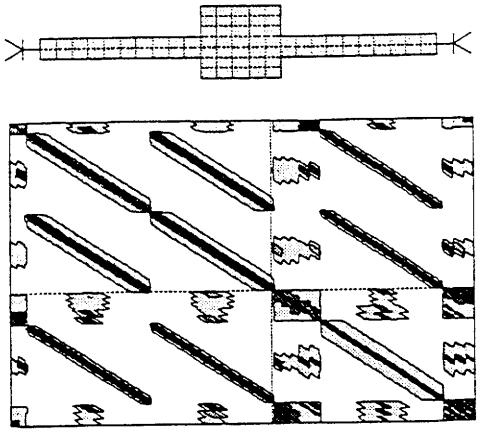

v_t	S	Solution Error	β Error	Scatt. Par. Error
10^{-7}	14.64 %	0.00 %	0.02 %	0.55 %
10^{-6}	35.97 %	0.02 %	0.05 %	0.96 %
10^{-5}	72.94 %	5.04 %	0.04 %	0.98 %
10^{-4}	85.71 %	5.61 %	0.07 %	1.95 %
10^{-3}	91.09 %	62.23 %	0.27 %	7.59 %
10^{-2}	92.7 %	212.64 %	3.17 %	22.58 %

Fig. 5. The layout of a double-stub, and the corresponding matrix pattern for different v_t values. In the table, the sparsity, solution error, and error in β and scattering parameters are shown for different v_t values.

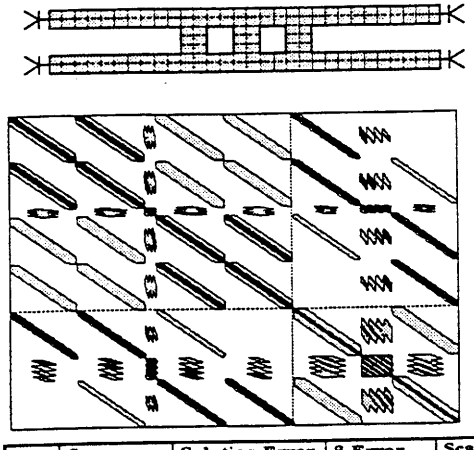

v_t	S	Solution Error	β Error	Scatt. Par. Error
10^{-7}	10.84 %	0.00 %	0.01 %	0.10 %
10^{-6}	35.41 %	0.07 %	0.04 %	0.24 %
10^{-5}	80.74 %	4.92 %	0.12 %	3.02 %
10^{-4}	93.61 %	8.14 %	0.50 %	3.83 %
10^{-3}	95.73 %	16.59 %	0.83 %	10.09 %
10^{-2}	96.55 %	143.03 %	3.71 %	34.31 %

Fig. 6. The layout of a branch-line coupler, and the corresponding matrix pattern for differentv_t values. In the table, the sparsity, solution error, and error in β and scattering parameters are shown for different v_t values.

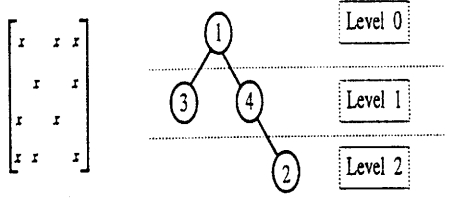

Fig. 7. Incidence graph and level partitioning for a given matrix.

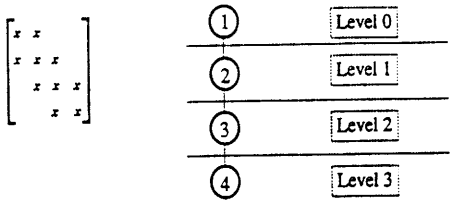

Fig. 8. Reordered matrix, corresponding incidence graph and level partitioning.